Unequally-spaced Waveguide Arrays for Silicon Nano-membrane-based Efficient Large Angle Optical Beam Steering

Amir Hosseini, *Student Member*, *IEEE*, David Kwong, Yang Zhao, Yun-Sheng Chen, and Ray T. Chen, *Fellow, IEEE*

Abstract— In this paper, we present a design methodology for silicon nano-membrane-based phased array structures with unequally-spaced elements for large angle optical beam steering. By optimizing a dielectric waveguide structure for transverse-magnetic polarized single mode operation at wavelength=1.55μm, we show that a one-stage optical phased array allows two-dimensional ±60° and ±45° optical beam scanning with minimal degradation in side-lobe-level and power efficiency. The number of array elements necessary to realize the desired array performance depends on the fabrication technique, which is formulated in the presented design methodology.

***Index Terms*—Laser beam steering, optical phased array, waveguide arrays, silicon.**

I. Introduction

Optical fiber phased arrays represent an enabling technology that makes possible simple, affordable, and lightweight laser beam steering with precise stabilization, random access pointing and programmable multiple simultaneous beams. Traditionally, optical beam steering has been achieved through mechanically controlled MEMS system [1] and liquid crystal (LC) based optical phased arrays (OPAs) [2]-[4]. Mechanical beam steering provides high steering efficiency and relatively large scanning angle. However, high precision rotating stages are required, which increase the device complexity and are not fast enough for high speed applications. LC OPAs provide rapid random access steering without the expensive and complex mechanical systems [5]. However, LC OPAs suffer from low steering speed (typically a few milliseconds response time) and limited steering angle (typically not more than 10°) [4]. A GHz optical beam steering system employing phased waveguide array was recently demonstrated with a maximum steering angle of about 6° [6]. The important issue with phased array waveguides is the strong coupling between the adjacent waveguides when the waveguide spacing is reduced to about one-half the operating wavelength, which is necessary for wide angle beam steering. Therefore, the optical coupling jeopardizes the side-lobe level and steering efficiency by imposing a lower limit on the waveguide spacing as will be discussed later in this paper. Other techniques such as beam steering with electro-wetting micro-prisms [7] and polymeric slab waveguide based thermally-induced beam steering [8] have response time in the order of tens of milliseconds.

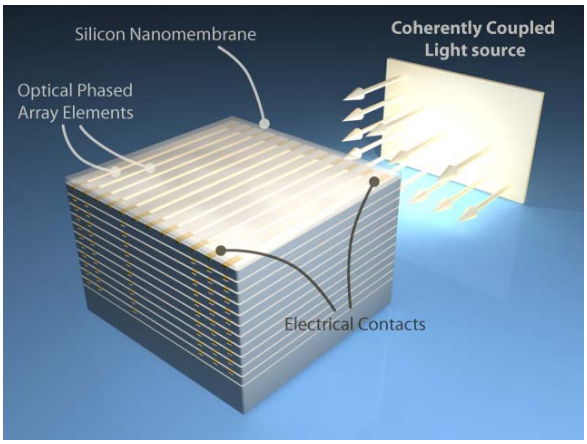

Fig. 1. A schematic of silicon nano-membrane-based OPA beam steering

So far, the large angle beam steering systems have been based on multi-stage systems combining LC OPAs with holographic glass and birefringent prisms [5], for which, alignment and packaging are very challenging.

In order to suppress the side-lobes at large steering angles, different unequally-spaced array structures were proposed [9], [10]. However, an unequally-spaced array realized by random placement of array elements [9] would not result in the optimum OPA performance. An array structure formed by gradually doubling the inter-element spacing along the array can suppress the side-lobes [10], but as we show, it severely reduces the steering efficiency. Additionally, the effects of optical radiator structure, finite fabrication accuracy and the achievable performance have not been investigated.

In this paper, we report a technique to minimize the side-lobe-level (SLL) in unequally-spaced optical phased waveguide arrays (USOPWAs) while achieving a steering angle of ±45°

Manuscript received Jan 1, 2009. This research is supported by the multi-disciplinary university research initiative (MURI) program through the AFOSR.

A. Hosseini, D. Kwong, Y. Zhao, Y. Chen and R. T. Chen are with the Microelectronic Research Center, Department of Electrical and Computer Engineering, University of Texas, Austin, TX 78758 USA (e-mail: ahoss@ece.utexas.edu; chen@ece.utexas.edu).

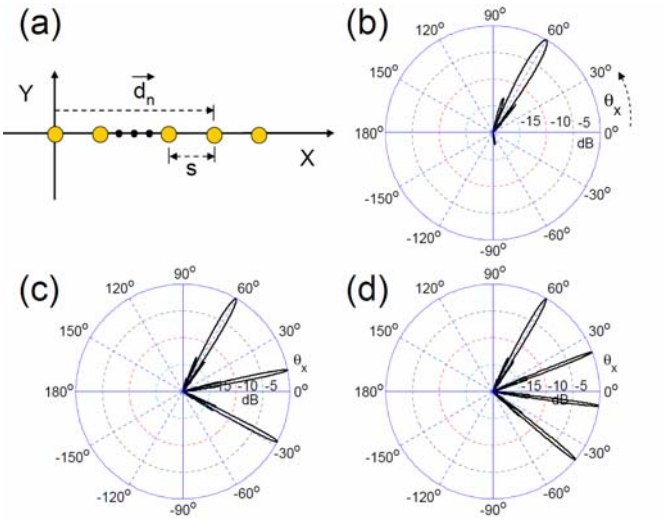

Fig. 2. (a) A schematic of a uniform 1D array. Array factor diagrams for 1D uniform arrays, assuming $\beta_n / |\vec{d}_n| = \frac{156^\circ}{(\lambda/2)}$, (b) N=32 and s=λ/2, (c) N=16 and s=3λ/2, (d) N=16 and s=2λ.

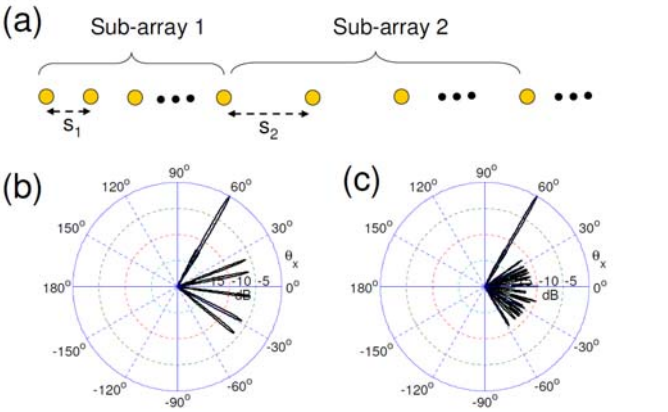

Fig. 3. (a) A schematic of the proposed (1D) USOPWA structure. Array factor diagrams for (b) M=2, N=32, q_1=3, q_2=4, s_0=λ/2, (β_2-β_1)/q_1=156° and (c) M=4, N=32 q_1=3, q_2=4, q_3=5, q_4=7, s_0=λ/2 and (β_2-β_1)/q_1=156°.

and avoiding the optical coupling by designing an unequally-spaced array composed of sub-arrays with non-overlapping grating lobes. By optimizing both the array structure and the individual waveguide structure, we present a design methodology for large angle optical beam steering with minimal performance dependence on the steering angle. Finally, we discuss the maximum performance achievable by USOPWAs and compare it with that of the other non-mechanical beam steering technique based on LC OPAs.

II. Unequally-scpaced Array Structure

A schematic of a silicon nano-membrane-based OPA system is shown in Fig. 1. Similar to their microwave counterparts, linear optical phased arrays consist of 1D or 2D arrays of single-mode waveguides operating at the designated wavelengths. The far field radiation (R) of an optical phased waveguide array (OPWA) is determined by the individual waveguide far field radiation (S), or the "envelope", as well as the array factor (A), $R(\theta_x,\theta_y)=A(\theta_x,\theta_y)\cdot S(\theta_x,\theta_y)$. At a given direction determined by a unit vector $\hat{r}$, the array factor is given as $A=\sum_{n=1}^{N} e^{j(\vec{K}\cdot\vec{d}_n+\beta_n)}$, where, $\vec{K}$ is the wave-vector ($\vec{K}=\frac{2\pi}{\lambda}\hat{r}$), and $\vec{d}_n$ is the translational vector of the nth radiator position, β_n is the input optical signal phase of the nth element, and λ is the wavelength. Beam steering can be done by changing the phase shift imposed on each array element. The total number of waveguides is N.

Consider a uniform 1D OPWA in the x-direction ($\vec{d}_n = ns\hat{x}$), as shown in Fig. 2(a). A criterion for determining the maximum inter-element spacing for the laser beam being steered to a given scan angle θ_{x0} (measured as the angle to the Z axis in the XZ plane), is to set the spacing so that the nearest grating lobe occurs at horizon [11], which leads to

$$\frac{s}{\lambda} \le \frac{1}{1+\sin\theta_{x0}}. \qquad (1)$$

This means that the spacing (s) should not be greater than one-half the wavelength for wide scanning angles. Figure 2(b) shows the array factor of a uniform 1D OPWA with s= λ/2, and the beam being steered at θ_{x0}=60°.

Although this requirement can be easily met in the case of microwave phased arrayed antennas, it imposes a fundamental limit in the case of OPWAs. Since optical waveguides can not support modal sizes smaller than one-half the wavelength, s=λ/2 spacing between adjacent optical waveguide would result in severe waveguide optical mode coupling and therefore, far field pattern (R) distortion.

In case of 1D arrays, $\vec{K}\cdot\vec{d}_n = \frac{2\pi|\vec{d}_n|}{\lambda}\sin\theta_x$. Considering β_n=0, for any s>λ, the grating lobes occur at $\theta_{xp}=\sin^{-1}\frac{P\lambda}{s}$, for P=±1, ±2 …, and s>|Pλ|. In the case of $\frac{\beta_n}{|\vec{d}_n|}=c$ (c is a constant), which is also the case in linear phased arrays, the main lobe occurs at $\theta_{x0}=\sin^{-1}\frac{c\lambda}{2\pi}$, independent of s, and the grating lobe angles are given by

$$\theta_{xp}=\sin^{-1}\left[\frac{P\lambda}{d}-\sin\theta_{x0}\right]. \qquad (2)$$

Now consider an unequally-spaced array consisting of *M* sub-arrays, where the sub-arrays themselves are uniform arrays with spacing $s_1=q_1s_0$, $s_2=q_2s_0$…and $s_M=q_Ms$, and q_i are integer numbers greater than or equal to two [see Fig. 3(a)]. If

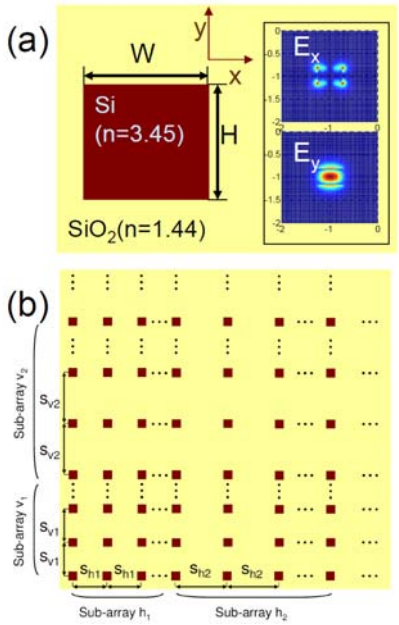

Fig. 4. (a) A schematic of a silicon nano-membrane waveguide; the fundamental TM mode field profiles are shown in the inset. (b) A 2D unequally-spaced optical phased waveguide array.

$\frac{\beta_n}{|\vec{d}_n|} = c$ is the same for all sub-arrays, the main lobes associated with all the sub-arrays occur at the same angle. Then if the greatest common divisor (gcd) of every q_i and q_j (i≠j) is 1, no two sub-arrays will have a common grating lobe angle according to (2). Thus, the main lobes of all the sub-arrays add up constructively, while there is no overlap between the peak grating lobes of each sub-array resulting in one a main lobe and some equi-ripple side-lobes. Although the side-lobe-level (SLL), defined as the ratio of the second largest lobe intensity to the maximum intensity (main lobe) [8], is 0dB for each sub-array, the total array factor can have a much smaller SLL.

To illustrate the idea behind the USOPWAs, consider two uniform 1D arrays with s=3λ/2 and s=2λ, for which the array factors are shown in Figs. 2(c) and 2(d), respectively. In each case there is at least one grating lobe in the array factor, and thus SLL=0. However, the grating lobes in Figs. 2(c) and 2(d) do not occur at the same angles and are narrow enough not to overlap. Placing these two uniform arrays along each other to form an unequally-spaced array with s_0=λ/2, q_1=3 and q_2=4, reduces SLL to -6dB as shown in Fig. 3(b).

In fact, for narrow enough sub-arrays' grating lobes, doubling the number of sub-arrays with non-overlapping grating lobes, can improve the SLL by 6dB. Obviously, the grating lobes corresponding to each sub-array can be arbitrarily narrowed by increasing the number of elements in each sub-array. Figure 3(c) shows the array factor of a USOPWA consisting of 4 sub-arrays with non-overlapping grating lobes. As will be discussed later, the lowest SLL achievable by this technique can not be better than that of a uniform array with s=s_0. For the USOPWA shown in Fig. 3(c), SLL decreases by increasing M, and finally saturates at the SLL of the far field diagram in Fig. 2(b) (SLL~-14dB).

Here we formulate the non-uniform array design methodology:

- *N*: the total number of radiators
- *M*: number of sub-arrays
- s_i: spacing in sub-array *i,* for *i*=1, 2…
- $s_i=q_i s_0$
  - fabrication resolution<s_0<λ/2
  - smallest possible integer numbers q_i such that: gcd(q_i,q_j)=1 (i≠j), and $q_1<q_2\ldots<q_M$
- s_1>modal size.

Note that s_0 must be smaller than λ/2 in order to avoid overlapping sub-array grating lobes. However, the lowest value of s_0 is determined by the fabrication process, or how precisely the waveguides can be placed in the array. In contrast, s_1 does not depend on the fabrication process, but is constrained by the optical coupling between the waveguides; In other words, s_1 must be large enough to avoid waveguide modal field profile overlaps. This condition automatically ensures no optical coupling in all the sub-arrays as well as the first one because $s_1< s_2\ldots< s_M$.

For example, in the case of the waveguide shown in Fig. 4(a), a center-to-center spacing of 2.4μm~1.5λ (for single mode operating waveguide dimensions W and H < 600nm at λ=1.55μm) diminishes the optical coupling between adjacent waveguides. Assuming, a fabrication resolution of 0.8μm [12], and therefore, s_0=0.8μm, we set s_1 and q_1 to be 2.4μm and 3, respectively. For M=2 [Fig. 3(b)], based on the design methodology described above, q_2=4. For M=4 [Fig. 3(c)], q_2, q_3 and q_4 are calculated to be 4, 5 and 7. Note, that once q_1 is calculated from s_0 and s_1, q_i values (i>1) need to be integer numbers with no common divisor (rather than 1) with each other or q_1 to avoid overlapping grating lobes. In addition, q_i values should be the smallest integer numbers possible to avoid unnecessary increasing of the number of side-lobes associated with each sub-array, which lowers the power efficiency (the ratio of the power radiated in the desired angle to the power radiated in all directions). Throughout the paper s_1=2.4μm and λ=1.55μm are assumed. Note that the presented non-uniform array structure is the first technique to address the optical coupling problem and finite fabrication precision at the same time.

The effect of modal size on the performance of an OPWA is two-fold. A lager modal size means narrower envelope and consequently, smaller allowable steering angles. Also, a larger modal size imposes a lower limit on the inter-element spacing in the array, and thus again, decreases the maximum allowable steering angles. The main importance of the proposed USOPWA design technique is that it allows the inter-element spacing in the array to be large enough to avoid coupling problems between adjacent waveguides, while at the same time still allowing large steering angles. In Section III we optimize the waveguide structure for the widest envelop at λ=1.55μm.

It is worth mentioning that ultra-small modal sizes (modal size<<λ/2) in plasmonic waveguides would allow for large

steering angles achievable by conventional uniform waveguide arrays. However, extremely high propagation loss (~0.3dB/μm) in plasmonic waveguides limits their applicability for practical devices [13], [14].

III. Optimized Waveguide Structure

Silicon-on-insulator (SOI) is an important component of fabricating high performance optical devices due to the high refractive index difference between Si (n=3.45) and SiO_2 (n=1.44). Fabrication of these single-crystal layers of Si on a buried oxide layer is commonly done using the Smart Cut method of hydrogen ion implantation. The ability to stack SOI layers may allow three-dimensional integration of optical devices. This can be accomplished through a number of methods. Alternating depositions of poly-crystalline Si and amorphous SiO_2 can be used, but these growth techniques allow for grain boundaries and surface roughening that contribute to optical degradation [15]. Extension of the Smart Cut method by multiple hydrogen ion implantations has been performed by Malevill et al. [16] but it requires multiple high temperature anneals and can be prohibitively expensive. Nanomembrane transfer is a simpler approach that does not require high temperature anneals, and yet still provides heterostructures with single-crystal Si films that contain high quality interfaces and low surface roughness [15]. In this method, multiple Si-nanomembrane OPAs can be stacked to allow 2D optical beam steering. Since 2D beam steering based on waveguide arrays requires 3D fabrication techniques, including stacking of layers of optical waveguide on top of each other, we assume a standard silicon process to estimate the performance of the USOPWAs (see Fig. 4).

A schematic of a silicon waveguide structure assumed here is shown in Fig. 4(a). A wider envelope allows for larger scanning angles. In order to calculate the envelope, we use Rsoft FEMSIM to generate the waveguide field profiles, and then we calculate the envelope $R = |E^2| \propto |E_\theta^2| + |E_\phi^2|$ using [17]:

(3)

$$E_\theta = j\frac{e^{-j\frac{2\pi}{\lambda}r}}{r\lambda}\left[\left(f_x\cos\phi + f_y\sin\phi\right) + \eta\cos\theta\left(g_y\cos\phi - g_x\sin\phi\right)\right]$$

$$E_\phi = j\frac{e^{-j\frac{2\pi}{\lambda}r}}{r\lambda}\left[\cos\theta\left(f_y\cos\phi - f_x\sin\phi\right) - \eta\left(g_x\cos\phi + g_y\sin\phi\right)\right]$$

$$\vec{f}(\theta,\phi) = \int \vec{E}_t(\vec{r})e^{j\vec{K}.\vec{r}}dr$$

$$\vec{g}(\theta,\phi) = \int \vec{H}_t(\vec{r})e^{j\vec{K}.\vec{r}}dr$$

where, $\vec{E}_t$ and $\vec{H}_t$ are the tangential electric and magnetic field components, and η=120π is the intrinsic impedance. The integrals are numerically computed over the waveguide cross-sectional plane. Also, note that $\cos\theta = \cos\theta_x\cos\theta_y$ and $\sin\phi = \sin\theta_x / \sqrt{\sin^2\theta_x + \sin^2\theta_y}$. Without loss of generality, we assume the waveguide is excited by the fundamental transverse magnetic (TM) input fiber mode, for which the main electric component is the y-direction [see Fig. 4(a) insets] [18].

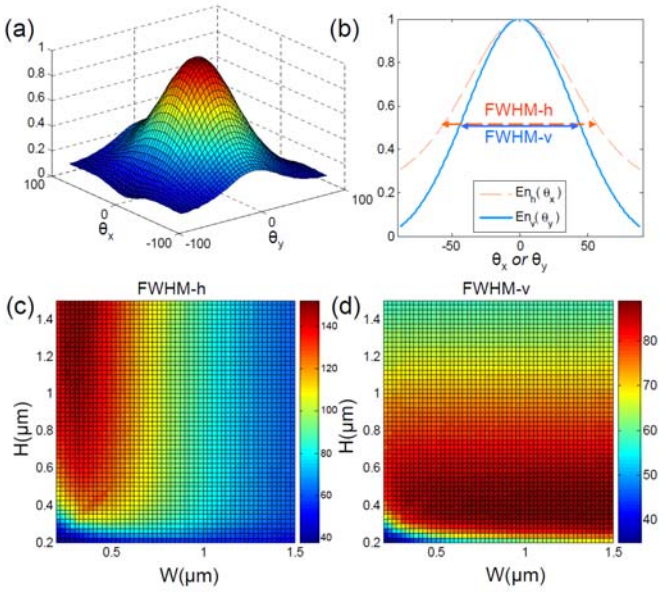

Fig. 5. (a) 2D far field radiation of the waveguide shown in Fig. 4(a) assuming W=500nm and H=350nm. (b) Horizontal (En_h) and vertical (En_v) envelopes as functions of θ_x and θ_y, respectively. (c) and (d) variations of FWHM of En_h and En_v [demonstrated in (b)], respectively, versus W and H depicted in Fig. 4(a). All the angles are in degrees and the envelope values in (a) and (b) are normalized.

A 2D far field radiation pattern (the envelope) is shown in Fig. 5(a). We define the horizontal [$En_h(\theta_x)$] and vertical [$En_v(\theta_y)$] envelopes as the variations of the far field radiation pattern at $\theta_y=0^\circ$ and $\theta_x=0^\circ$, respectively [Fig. 5(b)]. Figures 5(c) and (d) depict the full-width-half-maximum (FWHM) of $En_h(\theta_x)$ and $En_v(\theta_y)$, FWHM-h and FWHM-v, respectively, versus the waveguide width (W) and height (H). As the electromagnetic mode extents out of the waveguide area for W and $H \le 300nm$, the envelope becomes narrow (~40° in both directions). In the case of the TM mode, the field profile extent in the vertical direction is more than that in the horizontal direction [see Fid. 4(a) insets]. Thus the envelope is wider in the horizontal direction than in the vertical direction (FWHM-v<FWHM-h) [see Fig. 5(b)]. As the narrower envelope determines the worst case SLL and the power efficiency, the optimized waveguide dimensions should maximize FWHM-v, while maintaining single-mode condition, $W,H<\lambda/N_{eff}$, where, N_{eff} is the effective refractive index. From Figs. 5(c) and (d), we find that for W=500nm and H=350nm, the FWHM-h and FWHM-v values are 118° and 98°, which allow for about $|\theta_y|\le45^\circ$ and $|\theta_x|\le60^\circ$ beam steering in the vertical and horizontal directions, respectively, with maximum 3dB envelope variations. Based on the variations of the envelope in Fig. 5(a), we expect the worst-case array performance at $\theta_y=\pm45^\circ$ and $\theta_x=0^\circ$.

If the waveguide is excited by a TE mode, all the above arguments hold true if we replace x by y and horizontal by vertical and vice versa. In the next sections W=500nm and H=350nm are assumed.

IV. Optimized Array Design and Performance Analysis

A 2D generalization of the proposed USOPWA is shown in Fig. 4(b). For 2D arrays, the array elements are arranged in the XY plane, and similar to 1D cases θ_x (θ_y) is the angle to the Z axis in the XZ (YZ) plane.

We consider two parameters to evaluate the performance of the USOPWA, SLL and the power efficiency (PE), which is defined as the power in the main peak to the power radiated in all angles. For a fixed total number of radiators (N), as the number of sub-arrays (M) increases, the SLL decreases, however, since the overlap between the grating lobes of the sub-arrays increases, PE reduces. To find the optimum M that minimizes the SLL and maximizes the power efficiency, we define a dimensionless figure of merit (F) as

$$F = \frac{PE}{SLL}. \quad (4)$$

Note that s_0 is parameter determined by the fabrication process and therefore, we do not take it into account as an independent variable in the optimization process. PE can be numerically calculated by dividing the summation of the radiation field power within the FWHM of the peak in desired angle by the summation over the radiation field power in all directions.

Now, we consider two designs, Design I: s_0=800nm and Design II: s_0=50nm. In each case, we let N vary, and we find the M value that maximizes F for the worst case scenario (main peak of the steered beam at θ_{0y}=45° and θ_{0x}=0°). Note that 800nm and 50nm are conservative fabrication resolution assumptions for nano-imprint fabrication techniques and electron beam lithography, respectively [12]. The variations of F, the optimum M value, PE and SLL with N are shown in Fig. 6. The performance of Designs I and II for the non-steered beam is also depicted.

In Fig. 6(a) the curves corresponding to the steered beam, saturates as N increases, with some relatively small fluctuations. These fluctuations are due to the fact that any M value that is not a divisor of N is not acceptable. Therefore, as M fluctuates [see Fig. 6(b)] so does F.

A smaller s_0 allows for higher PE by reducing the number of grating lobes associated with each sub-array. Therefore, the performance of a USOPWA with a smaller s_0 suffers less from the falling envelope at large angles [Fig. 6(a)]. Furthermore, the optimum M is higher for a smaller s_0 as shown in Fig 6(b). Figure 7(a) shows that the degradation of PE from the non-steered beam compared to the worst case is only about 30% for both designs.

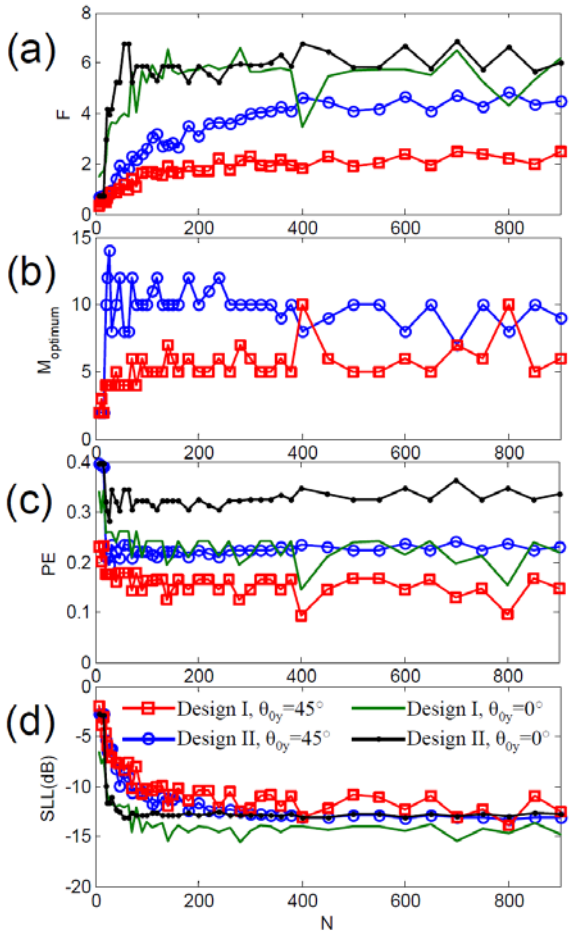

Fig. 6. Variations of the maximum figure of merit (F), the optimum M, power efficiency (PE), and side-lobe-level (SLL) versus N, in (a)-(d), respectively, for Design I (s0=800nm, q1=$\lceil s_1/s_0 \rceil$=3) and Design II (s0=50nm, q1=$\lceil s_1/s_0 \rceil$=48) for the beam steered at θ_{0y}=45° and θ_{0x}=0° and also non-steered beam (θ_{0y}=0° and θ_{0x}=0°). The optimum M is the same for both steered and non-steered beams in (b).

TA BLE I.
UNEQUALLY-SPACED ARRAY BASED BEAM STEERING PERFORMACE

Design	F-curve knee N value	M	Array size (μm)	θ_{0x}=0° θ_{0y}=0°		θ_{0x}=0° θ_{0y}=45°		θ_{0x}=60° θ_{0y}=0°	
				SLL(dB)	PE(%)	SLL(dB)	PE(%)	SLL(dB)	PE(%)
I	128	4	114	-12.1	26.3	-8.5	18.0	-9.0	21.0
II	64	8	300	-13.4	34.6	-9.4	23.4	-10.1	25.7

As the SLL of the array factor is independent from the steering angle (θ_0), degradation of the SLL with increasing the steering angle is mainly determined by the envelope. At small s_0 values, the side-lobes are more concentrated around the main lobe and therefore, degradation of the SLL as the steering angle changes becomes less significant as shown in Fig. 6(d). For the non-uniform array structure presented in [9], our calculations show a PE of 0.016, indicating that SLL was decreased at the expense of severe PE degradation. Based on Fig. 6(a), the F curves of the non-steered beam saturate at around N=128 and N=64 for Design I and II, respectively. Figures 7(a) and (b) depict PE and SLL values versus the steering angle (θ_{0x}=0° and varying θ_{0y}) at these knee N values of the F curves ({s_0=800nm, N=128, M=4} and {s_0=50nm, N=64, M=8}). Table I lists the SLL and PE values for these two designs at different steering angles.

Note that the steering efficiency, defined as the main peak intensity of the steered beam to the main peak intensity of the non-steered beam [4], is more than 65% in both cases at θ_{0x}=0° and θ_{0y}=45°. That is because in the case of USOPWAs,

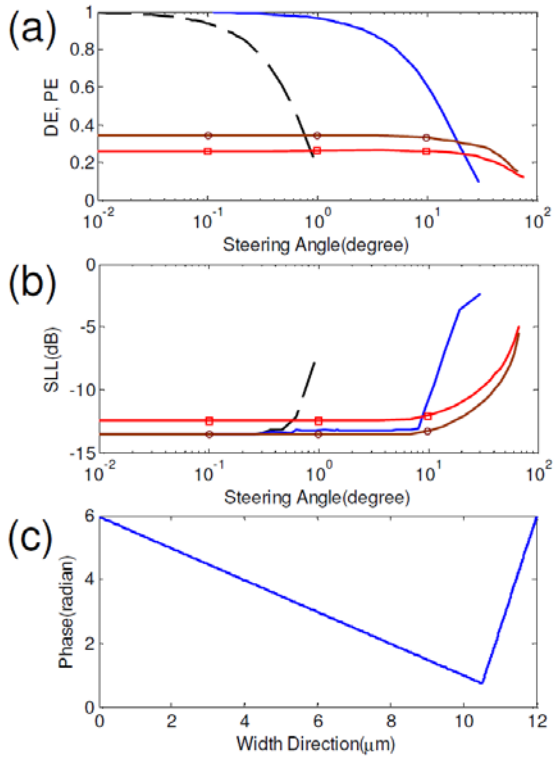

Fig. 7. (a) and (b), variations of the diffraction efficiency and SLL versus the steering angle for the liquid crystal (LC) based beam steerer; the black dashed line is for the device (w=20μm, L_f=10μm and maximum angle of 0.23°) from [3]; the blue solid line is the DE curve for the refractive-mode, high-Δn LC with optimized thickness and ideal phase profile (w=1.5μm, L_f=1.5μm, d=2.1μm, Δn=0.35) from [4]. Variations of PE and SLL for Design I (N=128, M=4) and Design II (N=64, M=8) with the steering angle in the vertical direction (θ_{0y}) are depicted by the squared and the circled lines, respectively. (c) Ideal phase profile assumed for the optimized LC OPA [the solid curve in (b) and (c)] with q=8.

the dependence of the steering efficiency on the steering angle is merely due to the envelope.

V. Comparison with Liquid Crystal Based Beam Steering Systems

Another category of nonmechanical, low power and low size-weight laser beam steering systems is the liquid-crystal optical phased array (LC OPA), with typical ~KHz speed, proposed by McManamon [4]. In terms of speed, OPWA systems (GHz) can outpace LC OPA systems (KHz) by orders of magnitude [6]. However, there are several applications for which LC OPAs are fast enough, such as laser radar, missile countermeasures, and free space laser communications [4]. Yet as mentioned before, limited steering angle is a remaining challenge for LC OPA laser beam steering. In every non-mechanical beam steering system proposed so far, as the steering angles increases, the appearance of the grating lobes increases the SLL and decreases the power efficiency. Proper voltage profile and electrode structure can increase the maximum steering angle of the LC OPA system. However, to what extent one can improve an LC OPA system performance has not yet been discussed. In this section we compare the theoretical performance of LC OPAs and USOPWAs at large angles. For LC OPAs, we consider the inevitable fly-back region, and assume an ideal linear phase profile and negligible fringing fields. For the USOPWAs, we consider both envelope and array factor effects, and assume an ideal phase distribution for the waveguides in the array.

We can compare the PE defined above with the diffraction efficiency (DE) reported from [3] and [4] for the LC OPAs, since the DE is the ratio of the power in the desired diffraction order to the total diffracted power. Figure 7(a) shows the variations of DE for a device from [3] and a reported optimized design from [4]. For the optimized reflective mode LC OPA structure (LC layer thickness d=2.1μm), high birefringence (Δn=0.35), both pixel size (w) and fly-back region size (L_f) of 1.5μm, and an ideal phase profile out of the fly-back region [Fig. 7(c)] are assumed. The DE curves in Fig. 7(a) were calculated from the analytical expression in [3]:

$$DE = \left(\frac{\sin \pi/q}{\pi/q}\right)^2 \left(1 - \frac{L_f}{qw}\right)^2 \quad (3)$$

Where, q is the number of pixels between two resets. When the beam is steered to 30°, DE is degraded more than 90% compared to the non-steered beam (steering efficiency less than 10%). Note that here, we have neglected the fringing field effects that distort the phase profile, specially, in the case of 2D beam steering, where the distorted phase profile in one direction can affect the phase profile in the other direction. Moreover, we assume that the fly-back region is limited to one pixel, and does not affect the phase profile of the period after the reset. Rather than the DE degradation problem, the SLL is also severely degraded at large steering angles in LC OPA. Fig. 7(b) depicts SLL as a function of the steering angle for the two abovementioned LC OPAs.

In order to estimate the theoretical limits of the LC OPA performance, we assume, a reflective LC with Δn=0.5, w/d=0.5 and L_f=w (a valid assumption for small pixel sizes), with the ideal phase profile. The steering angle is given as

$$\theta_0 = \sin^{-1}\left(\frac{2d\Delta n}{qw}\right) = \sin^{-1} 2/q\,, \quad (4)$$

Assuming q=4 and θ=30°, DE becomes 45%. Given that not more than ¾ of the power is radiated to the desired angle, the SLL will be no better an -6dB. Note that for w/d<1, the phase profile strongly deviates from the ideal ramp and that reduces the DE. In addition, 4 pixels are not enough to produce a desired phase profile. Therefore, the physical limits of the LC OPAs do not allow for an efficient beam steering at scanning angles larger than 30°. Also, $\Delta\theta_0/\Delta q \approx -2/\sqrt{q^2-1}$ becomes larger as q decreases (at large angles), and fundamentally, beam steering with a resolution better than about 5° is not possible at θ_0 more than 25° using single stage LC OPAs. Figures 7(a) and (b) show that the performance (DE, SLL and resolution) of the LC OPA strongly depends on the steering angle.

VI. Conclusions

In conclusion, we present an unequally-spaced OPA design for high-efficient large optical beam steering at 1.55μm, with minimal performance dependence on the steering angle. Assuming fabrication precision of 800nm and 128 array

elements, we demonstrate a beam steering with a worst-case power efficiency and side-lobe-level of about 18.0% and -8.5dB during ±60° and ±45° 2D optical beam steering, which correspond to degradation of about 32% and -3.6dB, respectively, with respect to those of the non-steered beam. Increasing the number of array elements and smaller fabrication resolution can improve the performance. The OPA performance dependence on the steering angle is only due to the far-field pattern of single elements, which can be further improved using waveguide structures that support smaller modal sizes.

VII. REFERENCES

[1] Y. Petremand, P.-A. Clerc, M. Epitaux, R. Hauffe, W. Noell, and N. F. de Rooij, "Optical beam steering using a 2D MEMS scanner", *Proc. SPIE*, vol. 6715, pp. 671502, Oct. 2007.

[2] P. F. McManamon, T. A. Dorschner, D. L. Corkum, L. J. Friedman, D. S. Hobbs, M. Holz, S. Liberman, H. Q. Nguyen, D. P. Resler, R. C. Sharp and E. A.Watson, "Optical phased array technology," *Proc. IEEE*, vol. 84, no. 2, pp. 268–298, Feb. 1996.

[3] X. Wang, B. Wang, J. Pouch, F. Miranda, J. Anderson, and P. Bos, "Performance evaluation of a liquid-crystal-on-silicon spatial light modulator," *Opt. Eng*., vol. 43, pp. 2769-2774, Nov. 2004.

[4] X. Wang, B. Wang, P. Bos, P. F. McManamon, J. J. Pouch, F. A. Miranda, and J. E. Anderson, "Modeling and design of an optimized liquid-crystal optical phased array", *J. Appl. Phys*., vol. 98, pp. 073101, Oct. 2005.

[5] P. F. McManamon, "Agile Nonmechanical Beam Steering," *Optics & hotonics News*, vol.17, pp. 24-29, Mar. 2006.

[6] M. Jarrahi, R. Fabian, W. Pease, D. A. B. Miller, and T. H. Lee, "High-speed optical beam-steering based on phase-arrayed waveguides*", J. Vac. Sci. Technol. B*, vol. 26, pp. 2124-2126, Dec. 2008.

[7] N. R. Smith, D. C. Abeysinghe, J. W. Haus, and J. Heikenfeld, "Agile wide-angle beam steering with electrowetting microprisms," *Opt. Exp*., vol. 14, pp. 6557-6563, 2006.

[8] G. Cocorullo, M. Iodice, "Thermally induced optical beam steering in polymeric slab waveguide". Fibres and Optical Passive Components, *Proc. of IEEE/LEOS*, 2005.

[9] F. Xiao, W Hu, and A. S. Xu, "Optical phased-array beam steering controlled by wavelength," *App. Opt*., vol. 44, no. 26, pp. 5429–543, Sept. 2005.

[10] J. H. Abeles and R. J. Deri, "Suppression of sidelobes in the far feld radiation patterns of optical waveguide arrays," *App. Phys. Lett.*, vol. 53, no. 15, pp. 1375-1377, Oct. 1988.

[11] R. J. Mailloux, *Phased Array Antenna Handbook*, 1993.

[12] H. Schift, "Nanoimprint lithography: An old story in modern times? A review", *J. Vac. Sci. Technol. B*, vol. 26, pp. 458-480, Mar. 2008.

[13] J. A. Dionne, L. A. Sweatlock, H. A. Atwater, and A. Polman, "Plasmon slot waveguides: Towards chip-scale propagation with subwavelength-scale localization", *Phys. Rev. B*, vol. 73, 035407, Jan. 2006.

[14] A. Hosseini, A. Nieuwoudt, Y. Massoud, "Optimizing Dielectric Strips Over a Metallic Substrate for Subwavelength Light Confinement", *IEEE photonic Tehnol. Lett,* vol. 19, no. 7, pp. 522 – 524, Apr 2007.

[15] W. Peng, M. M. Roberts, E. P. Nordberg, F. S. Flack, P. E. Colavita, R. J. Hamers, D. E. Savage, M. G. Lagally, and M. A. Eriksson, "Single-crystal silicon/silicon dioxide multilayer heterostructures based on nanomembrane transfer," *Appl. Phys. Lett.*, vol. 90, 183107, May 2007.

[16] C. Maleville, T. Barge, B. Ghyselen, A. J. Auberton, H. Moriceau, and A. M. Cartier, "Multiple SOI layers by multiple Smart-Cut (R) transfers," *Proc. of IEEE International SOI Conference*, Wakefield, p. 134, 2000.

[17] S. J. Orfanidis, *Electromagnetic Waves and Antennas*, 2004.

[18] Y. Vlasov and S. McNab, "Losses in single-mode silicon-on-insulator strip waveguides and bends," *Opt. Exp.* ,vol. 12, pp. 1622-1631, 2004.

Amir Hosseini (S'05) received his B.Sc. degree (with honors) in electrical engineering in 2005 from Sharif University of Technology, Tehran, Iran, and the M.S. degree in electrical and computer engineering in 2007 from Rice University, Houston, TX. He is currently working toward his Ph.D. degree in Optical Interconnect Group at The University of Texas at Austin, Department of Electrical and Computer Engineering. He is engaged in research on optical phased array technology and high performance optical modulators design and optimizations. His main focus is on the design optimization for nano-scale manufacturability.

David Kwong received his BS degree in electrical engineering in 2006 from the University of Texas at Austin. He is currently pursuing his Master's Degree with the Optical Interconnect Group at UT Austin, with a focus on optical phased array technology and optical modulation. Before joining UT Austin, Kwong spent two years working at Samsung Austin Semiconductor in process integration for DRAM Back End Of Line (BEOL) processes.

Yang Zhao received her M.S. degree in Optics in May 2008 from College of Optics and Photonics-CREOL, the University of Central Florida. She is currently working toward her PhD degree at the department of Electrical and Computer Engineering, the University of Texas at Austin. Her current research interest is focused on Si photonics, optical phased array and nano-fabrication.

Yun-Sheng Chen received his M.S. degree in Optics from the College of Optics and Photonics-CREOL, the University of Central Florida. He is currently working towards his Ph.D. degree at the department of electrical and computer engineering, University of Texas at Austin. His research interest is focused on photonic crystal waveguide, optical true time delay, and nano-fabrication.

Ray T. Chen (M'91–SM'98–F'04) holds the Cullen Trust for Higher Education Endowed Professorship at UT Austin and the director of nanophotonics and optical interconnects research lab within the microelectronics research center. He is also the director of a newly formed AFOSR Multi-disciplinary Research Initiative (MURI) Center for Silicon Nanomembrane involving faculty from Stanford, UIUC, Rutgers and UT Austin. He received his BS degree in Physics from National Tsing-Hua University in 1980 in Taiwan and his MS degree in physics in 1983 and his PhD degree in Electrical Engineering in 1988, both from the University of California. He joined UT Austin as a faculty to start optical interconnect research program in the ECE Department in 1992. Prior to his UT's professorship, Chen was working as a research scientist, manager and director of the Department of Electrooptic Engineering in Physical Optics Corporation in Torrance, California from 1988 to 1992. Chen also served as the CTO/founder and chairman of the board of Radiant Research from 2000 to 2001 where he raised 18 million dollars A-Round funding to commercialize polymer-based photonic devices. He also serves as the founder and Chairman of the board of Omega Optics Inc. since its initiation in 2001. Over 5 million dollars of research funds were raised for Omega Optics. His research work has been awarded with 94 research grants and contracts from such sponsors as DOD, NSF, DOE, NASA, the State of Texas, and private industry. The research topics are focused on three main subjects: 1. Nano-photonic passive and active devices for optical interconnect applications, 2.Polymer-based guided-wave optical interconnection and packaging, and 3. True time delay (TTD) wide band phased array antenna (PAA). Experiences garnered through these programs in polymeric material processing and device integration are pivotal elements for the research work conducted by Chen's group. Chen's group at UT Austin has reported its research findings in more than 510 published articles including over 80 invited papers. He holds 18 issued patents. He has chaired or been a program-committee member for more than 90 domestic and international conferences organized by IEEE, SPIE (The International Society of Optical Engineering), OSA, and PSC. He has served as an editor, co-editor or coauthor for 22 books. Chen has also served as a consultant for various federal agencies and private companies and delivered numerous invited talks to professional societies. Dr. Chen is a Fellow of IEEE, OSA and SPIE. He was the recipient 1987 UC Regent's dissertation fellowship and of 1999 UT Engineering Foundation Faculty Award for his contributions in research, teaching and services. He received IEEE Teaching Award in 2008. Back to his undergraduate years in National Tsing-Hua University, he led a university debate team in 1979 which received the national championship of national debate contest in Taiwan. There are 32 students who received the EE PhD degree in Chen's research group at UT Austin.